Numerical Simulation of Air Flow around the NP01 Car Using the Realizable k-ε Turbulence Model to Predict Aerodynamic Forces and Moments

M. Siavashi[1,*], M. H. Shojaeefard[2]

1 Assistant Professor, School of Mechanical Engineering, Iran University of Science and Technology 2 Professor, School of mechanical Engineering, Iran University of Science and Technology

Abstract

In this study, a numerical computational fluid dynamics study is conducted in order to predict the aerodynamic forces on the NP01 car. The turbulent air flow around the car is modeled using the realizable k-ε model. First, results are validated against those presented for the Ahmed's body. Next, the fluid flow around the car is simulated for different car speeds (60 to 100 mph) and flow directions (0 to 20 degree) and the drag and lift forces and coefficients are calculated. Increasing the car speed leads to increase of the drag and lift forces. While, the drag and lift coefficients of the car for all studied speeds are almost constant and are respectively equal to 0.32 and 0.11. In addition, for different flow directions the drag coefficient would increase up to 0.45. Also, the effect of mirrors on the drag force is investigated. Results reveal that removing the mirrors leads to approximately 11% reduction in the drag force with no significant reduction in the drag coefficient. Furthermore, the effect of car elevation on the drag and lift forces is analyzed. It has been shown that when the car elevation decreases up to 25 mm, the drag force will decrease more than 7%, and the drag and lift coefficients are still constant. Keywords: road sign detection, text detection, object detection from video, fuzzy logic, MSER

Keywords*: Aerodynamics, realizable k-ε, turbulence, numerical simulation, drag, lift.*

Introduction

Design and analysis of different systems of a car necessitates to know forces and moments which are acting on these systems. When a car is running on the road, two main forces are acting on that: 1- the forces caused by the interaction of the car with the road; and 2- the aerodynamic forces due to the air flow around the car. Aerodynamic forces and moments in the Cartesian coordinate are divided into three principal components. Force components are known as the drag, lift and side forces, and the moment components are categorized as the yawing, pitching and the rolling moments. These forces and moments can be estimated using a wind tunnel test [1,2]. However, this test is very expensive and is limited to the operating conditions of the wind tunnel. Computational fluid dynamics (CFD) is the second proper choice that can be employed to provide an estimation of the aerodynamic characteristics of a car with a substantially cheaper cost [3].

Numerous research studies have been devoted to numerical simulation of aerodynamic forces on automotives [4–6]. All these works start with the mathematical formulation of the governing equations of turbulent fluid flow around the car and ends to numerical solution of these equations. Different mathematical and numerical techniques are developed to solve the turbulent flow around vehicles. Solution of Reynolds-averaged Navier-Stokes equations (also known as RANS) is the most traditional method of solving turbulent flows. In order to model the turbulent viscosity in these equations, different classical turbulence models have been introduced and are categorized into: 1- zero equation model (mixing length model); 2- one equation model (Spalart-Almaras); 3- two equation models (such as k-ε and k-ω models); and 4-seven equation model (RSM). In addition to the RANS-based methods, which solve the time-averaged form of Navier-Stokes equations and are commonly used in industrial applications, DNS and LES methods have also been developed for turbulent flow simulations [7]. These two later

methods are more accurate than the RANS methods, however they are computationally expensive techniques and their costs prohibit simulation of practical engineering problems.

The RANS methods are now commonly used for simulation of practical engineering problems and among them the k-ε model is the most distinguished one. Improvements have been made in this model to promote its performance, and different k-ε models have been developed yet. The standard k-ε model was proposed by Launder and Spalding [8], then Yakhot and Orszag [9] extended it to the RNG model, and Shih et al. [10] developed the realizable k-ε model. The realizable k-ε model uses a new formulation for the turbulent viscosity. In addition, a new transport equation for the dissipation rate of ε is implemented in this model. This model covers the weaknesses of the old ones and can resolve accurately the spreading rate of both planar and round jets. This model is also capable to make proper prediction for the problems including adverse pressure gradients, separation and recirculation.

The RANS models have been implemented in many different research works to predict aerodynamic forces on automotive vehicles. Blocken and Toparlar [11] presented results of CFD simulations and wind tunnel measurements to investigate influences of a following car on a cyclist drag. They used the standard k-ε model and validated these results against experimental measurements. Murad et al. [12] used a CFD and a computational aero-acoustics code to simulate fluctuating air flow and the noise propagation in the A-pillar region of a vehicle. They employed the standard k-ε turbulence model in their study. Wang and Hu [13] used the standard and the RNG k-ε models in order to predict the drag and lift coefficients of the Ahmed standard car [14] model. They concluded that the RNG k-ε model is more precious than the standard one. Bella and Krastev [15] performed a numerical study of flow around the Ahmed body, using several RANS turbulence models, as well as different wall treatments. They showed that the realizable k-ε model is more accurate than the RNG k-ε model and returns sufficiently close results to the experimental drag. Multiple research works [16,17] suggested to employ the realizable k-ε RANS model for aerodynamics study of cars. McManus and Zhang [18] showed that among the two-equation turbulence models, the realizable k-ε model is the best representation of them. Recently, Dang and Chen [19] investigated the influence of wheel rotation on the aerodynamic characteristics of a race car using the realizable k-ε model.

NP01 is the first prototype of the national platform of a sedan car designed in Iran University of Science and Technology. In this study, in order to find the aerodynamic forces and moments on NP01 car, fluid flow around the car is simulated numerically using the FLUENT code. Turbulence is modeled implementing the realizable k-ε model and effects of flow speed, flow direction (or yawing angle), car elevation, and mirrors on aerodynamic characteristics of the car have been investigated precisely. Finally, results are presented in terms of the force and moment components, and their pertinent non-dimensional coefficients.

Problem Description

Geometrical description

Schematic of a car and the coordinate system with the force and moment components are illustrated in **Error! Reference source not found.**. In this figure, WB is the wheelbase distance. Cd, Cl and Cs are respectively the drag, lift and side force coefficients. Crm, Cpm and Cym indicate the rolling, pitching and yawing moment coefficients, respectively.

For CFD simulation of flow around the car, the full scale model of the car is used. The geometry of the car is exhibited in **Error! Reference source not found.**. The original model contains many complexities and should be simplified and smoothed in order to make a high quality mesh for numerical simulation. As can be seen in **Error! Reference source not found.**, there are some sharp edges and very short curves in the original model, which are merged into each other to make a smooth model. The length, width and height of the car are approximately L×W×H= 4.2×1.7×1.5 m3. The frontal area of the car (Af) – defined as the vehicle area projection in the x-direction – is 2.184 m2 at the base level. When the ride height lowers by 25 mm or the mirrors are removed the frontal area decreases to 2.169 m2 and 2.133 m2 respectively. The wheelbase distance (WB) equals 2.6 m.

Testing conditions and flow parameters

The working fluid is assumed to be air with the density of $\rho = 1.225\ \mathrm{kg/m^3}$ and viscosity of $\mu = 1.79 \times 10^{-5}\ \mathrm{kg/m.s}$. Also it is supposed that the car surface roughness is zero. Numerical simulations are conducted in four main configurations (as explained in Table 1) to measure the standard 3 forces (drag, lift and side forces) and 3 moments (yaw, roll and pitch moments).

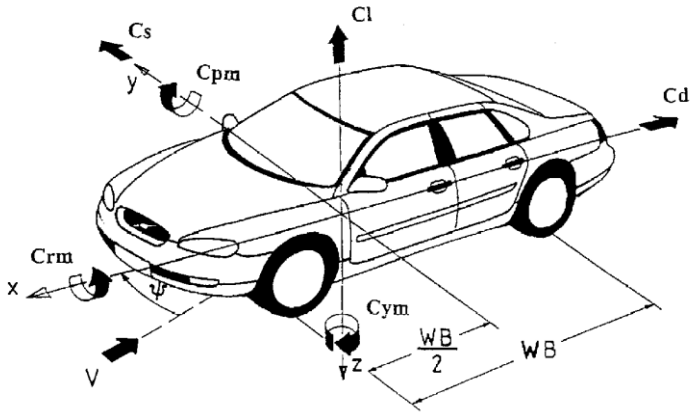

Fig1. A schematic of axes system and the force and moment components.

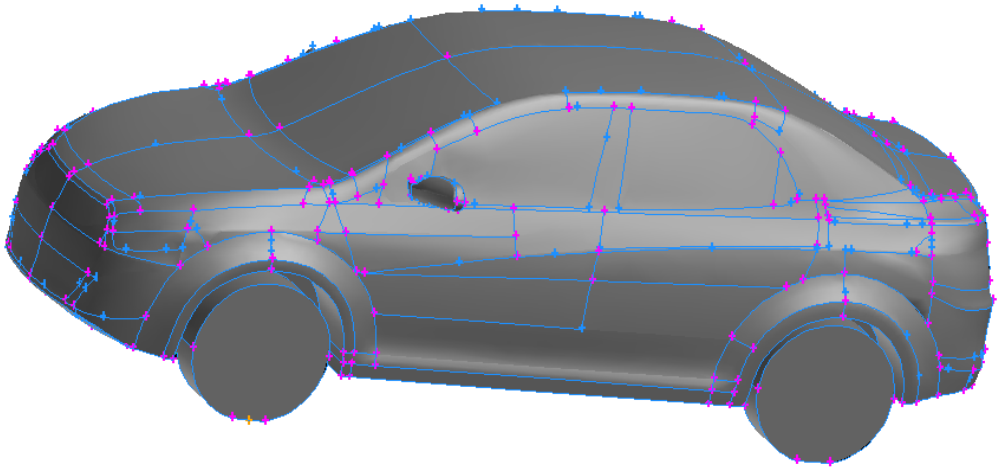

Fig2. The simplified and smoothed geometry of the car.

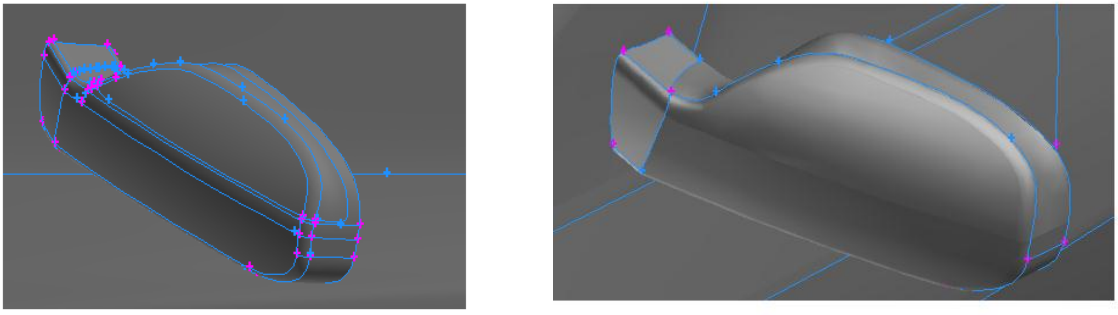

a) b)

Fig3. Mirror of the car model, a) the original model, and b) the smoothed model.

Table 1 Different aerodynamic numerical simulation configurations of the car.

Test No.	Parameter study	Velocity (mph)	Yaw ψ (°)	Description
1	Car speed	60 70 80 90 100	0	
2	Side wind	80	0 5 10 15 20	
3	Elevation	80	0	Lower ride height up to 25 mm
4	Mirrors	80	0	Remove the mirrors

In the first test category, the car is fixed in its base level and the yaw angle (ψ) – the angle between the vehicle body longitudinal axis (x-direction) and the component of the relative air velocity vector in the x-y plane – is zero. Then the effect of velocity speed on forces and moments will be studied. Numerical simulation will be performed for the five, 60, 70, 80, 90 and 100 mph flow speeds. In the second configuration, the effect of yaw angle on the forces and moments will be investigated. The third configuration is devoted to the effect of elevation of the ride height of the car, and the fourth test is conducted for a car with removed mirrors to find the effect of mirrors on aerodynamic characteristics of the car.

Numerical Simulation

The steady-state, incompressible, turbulent flow of air around the car is solved numerically. The RANS equations in conjunction with the realizable k-ε equations are solved for numerical simulation of the problem. Transport equations for k and ε in the realizable k-ε model are as follows:

$$\frac{\partial}{\partial x_j}\left(\rho k u_j\right)=\frac{\partial}{\partial x_j}\left[\left(\mu+\frac{\mu_t}{\sigma_k}\right)\frac{\partial k}{\partial x_j}\right]+G_k+G_b+\rho\varepsilon+ \tag{1}$$

$$\frac{\partial}{\partial x_j}\left(\rho\varepsilon u_j\right)=\frac{\partial}{\partial x_j}\left[\left(\mu+\frac{\mu_t}{\sigma_\varepsilon}\right)\frac{\partial \varepsilon}{\partial x_j}\right]+\rho C_1 S\varepsilon-\rho C_2+\frac{\varepsilon^2}{k+\sqrt{\upsilon\varepsilon}}+C_{1\varepsilon}\frac{\varepsilon}{k}C_{3\varepsilon}G_b \tag{2}$$

$$C_1=\max\left[0.43,\frac{\eta}{\eta+5}\right],\qquad \eta=S\frac{k}{\varepsilon},\qquad S=\sqrt{2S_{ij}S_{ij}} \tag{3}$$

In the above equations, Gk and Gb represent the generation of turbulent kinetic energy due to the mean velocity gradients and buoyancy, respectively. C1ε, C2, σk and σε are empirical constants set as:

$$C_{1\varepsilon}=1.44,\ C_2=1.9,\ \sigma_k=1.0,\ \sigma_\varepsilon=1.2 \tag{4}$$

More details about the realizable k-ε equations are represented in [10].

Numerical setup

To solve the governing equations numerically, FLUENT uses a finite volume discretization scheme. A pressure-based solver is implemented and a second order approximation is used for the convective and viscous terms of the RANS. Enhanced wall treatment has also been used for viscous sub-layer solution over the car surface. To handle the pressure-velocity coupling, the SIMPLE algorithm is employed [20]. The convergence criteria of residuals of the governing equations are set to lower than 10-4.

Computational domain and boundary conditions

The computational domain is considered as a cube and the car volume is subtracted from this cube. The size of the computational domain should be selected in a manner that the boundaries cannot affect the flow around the car. Therefore, as exhibited in **Error! Reference source not found.**, a 10 m length exists in front of the car and the longer length of 25 m exists at the back of car. The width and height of the domain are respectively 9 m and 8 m. The overall size of the domain is L×W×H=40×9×8 m3.

In order to solve the problem with a higher computational speed, it is suggested to have a structured grid. Hence, the computational domain is divided into 60 sub-regions. A sub-region contains the car and a tetrahedral unstructured grid is generated in this region around the car. The other 59 sub-regions are segmented with structured grids.

Defined boundary conditions of the computational domain are illustrated in **Error! Reference source not found.**. The inlet plane, where the airflow enters, is considered to be a velocity-inlet boundary with defined velocity vector. The outlet plane, where the airflow exits, is considered to be a pressure-outlet boundary with zero gauge pressure. The floor is defined as a moving wall with the same speed of the flow inlet. All the car surfaces are defined as stationary walls, except the tires which have a rotational speed. The top wall and side walls of the domain are defined as symmetry to make sure that flow can slip on them and cannot cross through them. The turbulent intensity of the inflow and the back flow is set to 1 percent.

Mesh generation and independency check

In order to solve the transport equations, a computational mesh is required to be generated in the computational domain. To meet this need, mesh generation is conducted using Gambit software. To produce a high quality mesh in the 3D domain, first a 2D unstructured grid is generated on the car surface and then it has been extended to the 3D domain. **Error! Reference source not found.** shows a sample generated 2D mesh on the car surface.

To estimate the boundary layer with precise accuracy a fine grid has to be generated on the car surface. Hence, ten prism layers that overlap at the surface of the model are used. The prism layers' configurations are adjusted in a trial procedure to confine y+ in the range of 30<y+<300, when using the enhanced wall treatment. y+ is a non-dimensional distance from the wall and is defined according to the following relation:

$$y^+ = \frac{\rho u_\tau y}{\mu} \tag{4}$$

where y is the distance from the wall and uτ is the friction velocity. **Error! Reference source not found.** shows the generated mesh in the mid-plane of the car, and the prism mesh layers are highlighted in the vicinity of the car surface.

A grid independency check has also been performed to produce independent results from the computational grid. The effect of the computational grid on the drag coefficient is studied for different number of grid cells and results are presented in **Error! Reference source not found.**. As can be seen, a grid with approximately 2.5 million cells represents the same drag coefficient as the grids with 4 and 6 million cells. Hence, the generated grid with 2.5 million cells is a proper mesh for numerical simulation of the problem.

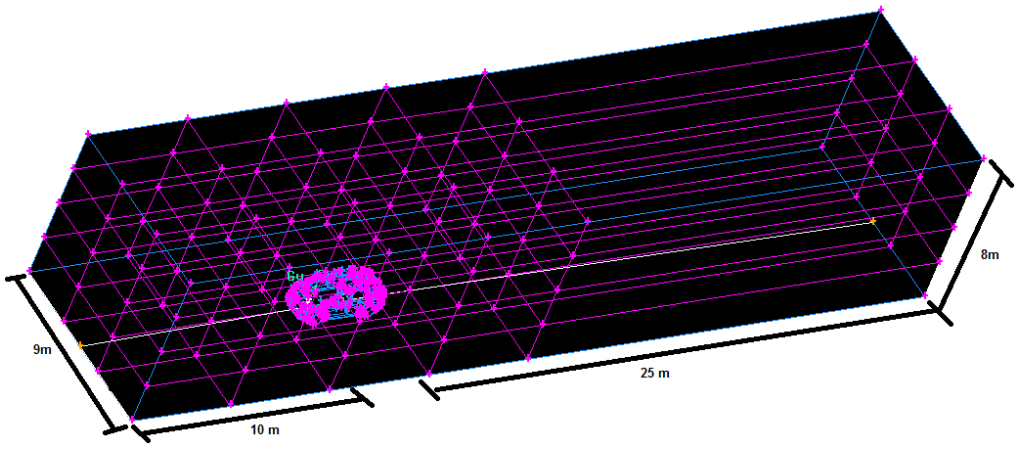

Fig4. The computational domain and the position of car in this domain.

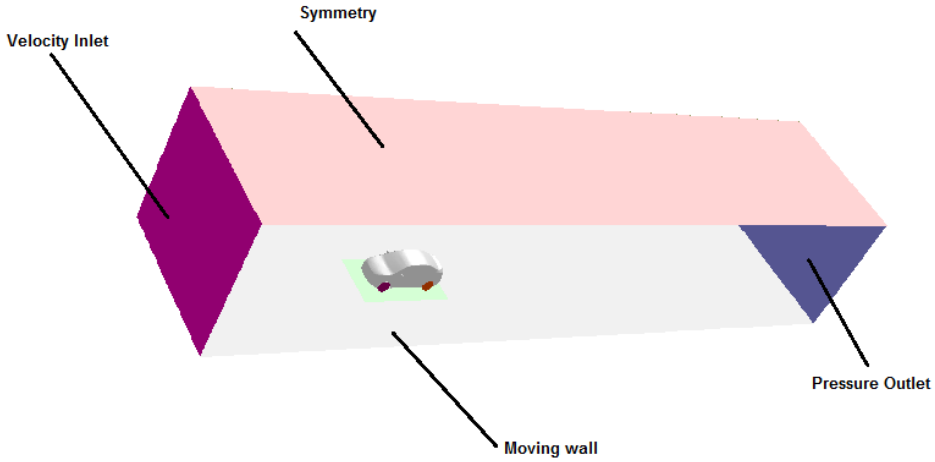

Fig5. Boundary conditions of the computational domain.

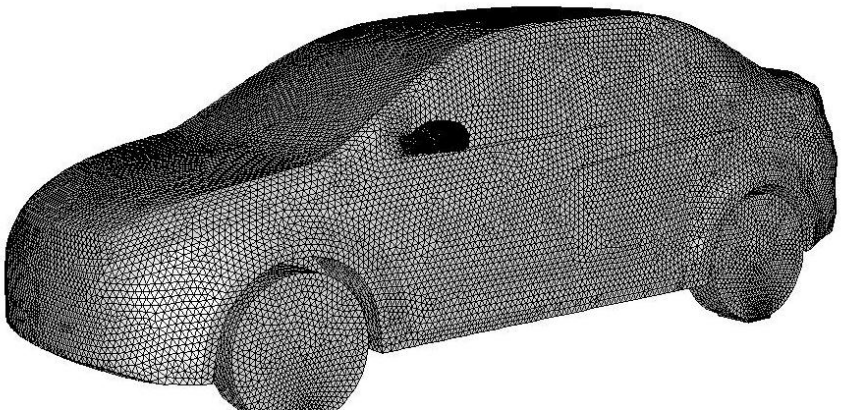

Fig6. A sample 2D unstructured grid on the car surface

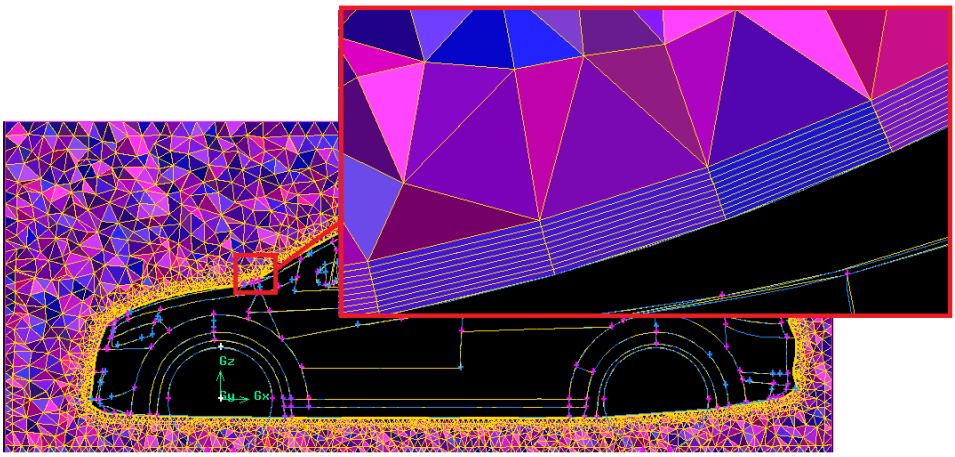

Fig7. The mesh generated around the car and the prism layers near the car surface.

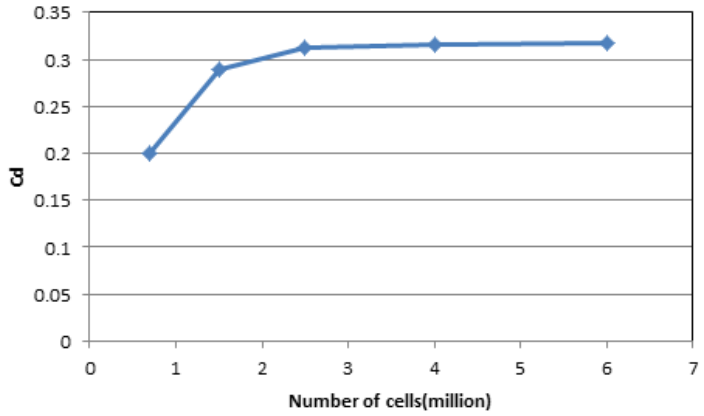

Fig8. Drag coefficient (Cd) independency check from the computational grid.

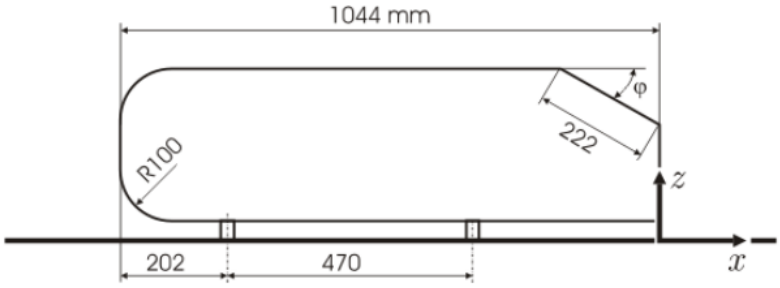

Fig9. The Ahmed model introduced for code validation (units in mm).

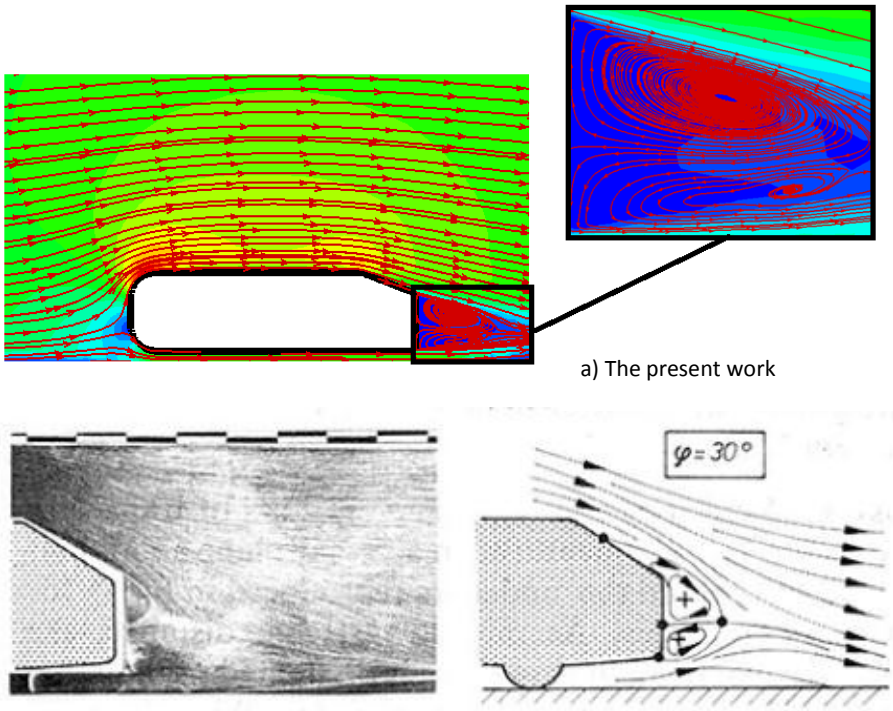

a) The present work

b) Wind tunnel results by Ahmed [21]

Fig10. Comparison between results of the present work and those obtained from wind tunnel by Ahmed [21].

3.4 Validation

To make sure that the settings of the numerical simulator has been done properly, first a numerical simulation is performed on the reference Ahmed model using the same numerical settings as the main problem. The standard Ahmed model is exhibited in Fig. 9 and a 2D numerical simulation is conducted for this model when the flow speed is 40 m/s.

A comparison between results of the present study – in terms of streamlines in the wake region – and those obtained by Ahmed [21] from the wind tunnel is exhibited in **Error! Reference source not found.**. It is observed that the wake region in the back of the model is presented properly.

Another comparison is made for predicting the lift and drag coefficients, and results are compared with those of Beaudoin and Aider [22], as explained in Table 2.

As can be seen, the present work results, with an acceptable error, could fit to results of reference [22].

Results and discussion

Results are presented in the next sub-sections, first different aerodynamic phenomena happening around the car are investigated. Afterward, in the next sub-sections effects of velocity, cross wind, ride height and mirrors on force and moment components are explained and discussed.

Flow visualization and aerodynamic characteristics

Streamlines are the lines which are tangential to the flow velocity. **Error! Reference source not found.** exhibits the streamlines which are launched from a surface in front of the car's mirror. As can be seen, the streamlines are in direction with the car surface and some streamlines tend to bend toward the rear side of the car. Also the wake region in the back of the car can be observed clearly.

Formation of the wake region in the back of blunt bodies leads to low pressure regions which increases the pressure drag force. To visualize the flow in the back of mirrors, Fig. 1 illustrates the streamlines around the mirror. As is expected, a wake region is formed in the back of the mirror, and this wake region could be predicted properly with the numerical solver.

Integration of the pressure distribution on the car surface leads to the pressure drag and lift forces. **Error! Reference source not found.** shows contours of pressure distribution on the car surface. Red regions are high pressure and the blue regions are low pressure. Clearly, the car front and the front of mirrors are high pressure regions with the maximum pressure values.

Velocity vectors around the car in the longitudinal symmetric plane of the car are represented in **Error! Reference source not found.**. A stagnant point can be detected in front of the car, which is placed in the high pressure zone exhibited in **Error! Reference source not found.**. In the stagnation point the flow around the car is split into two streams and flows upward and downward. A vortex area has also formed in the back of the car trunk.

Table 2 Comparison of the lift and drag coefficients.

Coeff.	Present work	Beaudoin and Aider [22]	error
Lift	0.337	0.351	3.98%
Drag	0.452	0.461	1.95%

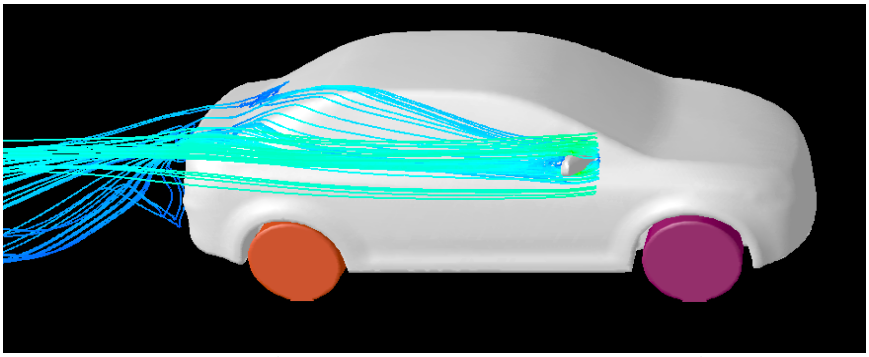

Fig11. Streamlines after the mirror: streamlines bend to the rear side of the car.

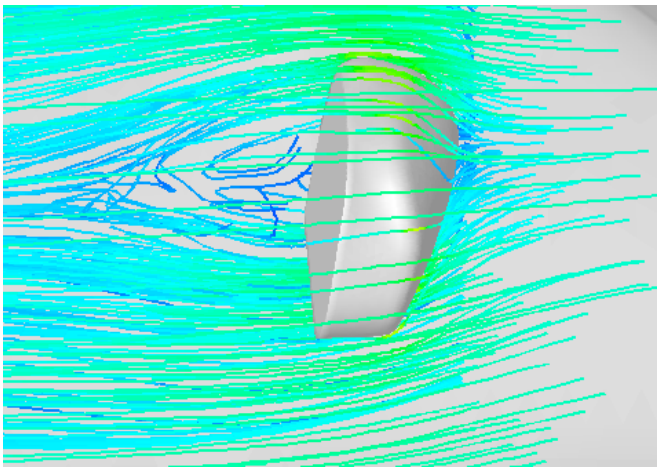

Fig. 1 Streamline after the mirror: a wake region is formed on the back of mirror.

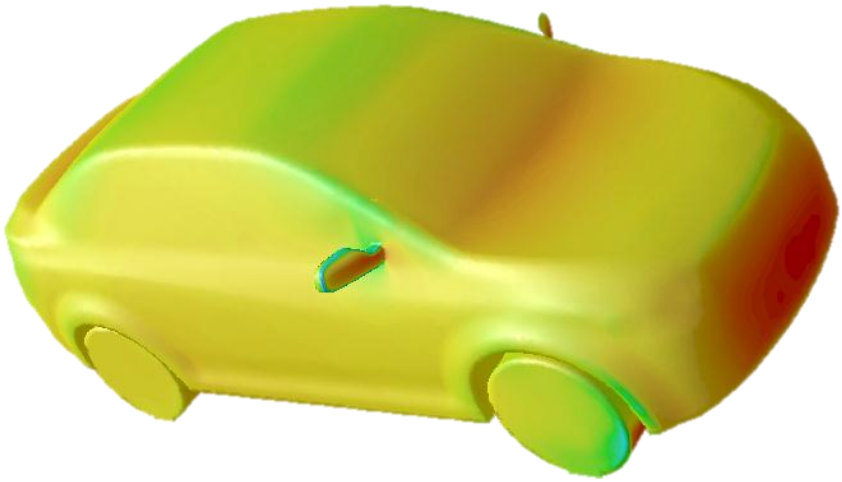

Fig12. Contours of pressure distribution on the car surface

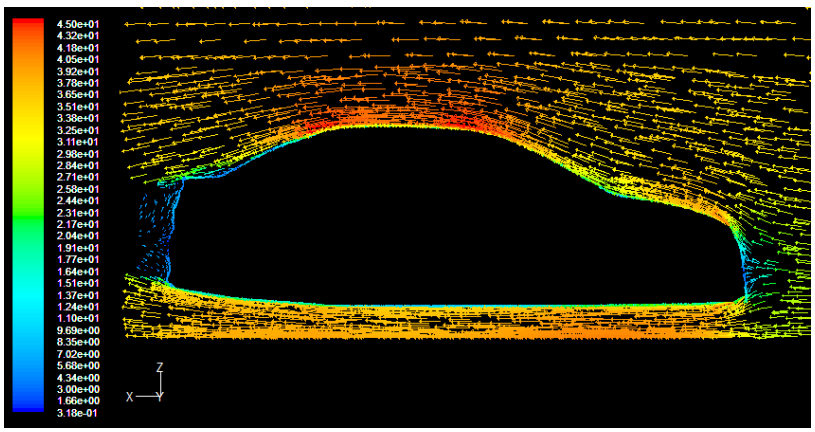

Fig13. Velocity vectors around the car presented in the mid-plane surface.

Fig. 15 depicts the streamlines in the longitudinal symmetric plane. The density of streamlines of the flow stream under the car is higher than top of the car. Also in the wake region downstream of the car, a pair of recirculating regions is formed. These recirculating zones are generated by separation of the flow from the car bottom surface, and also the interaction of the under stream flow with the flow caused by the rotation of wheels.

Error! Reference source not found. illustrates velocity vectors around the car in the x-y plane, and focused on the vortex region downstream the car. As exhibited, separation of flow stream from the side surfaces of the car forms wake regions after the car trunk.

Streamlines in the vicinity of car tires are represented in **Error! Reference source not found.**. Since the flow toward the car and the flow due to rotation of tires are opposite to each other, a stagnation point is detected on top of the tire.

Aerodynamics forces and moments

Aerodynamic forces and moments are the main parameters which are used for analysis of different car systems. In the present section, the effect of different parameters on the aerodynamic forces and moments and their pertinent coefficients are discussed.

Speed effect

First the effect of the car velocity, in its base condition, on force and moment components is explained. The drag (D), side (S) and lift (L) forces, and the rolling (RM), pitching (PM) and yawing (YM) moments on the car are summarized in Table 3. As a consequence of symmetry of the car and the flow around it, the side force and RM and YM are zero. Also, as expected, the drag and lift forces increases with increasing the velocity. The lift force is positive that acts to lift up the car from the road, however its value in comparison to the car's weight is negligible.

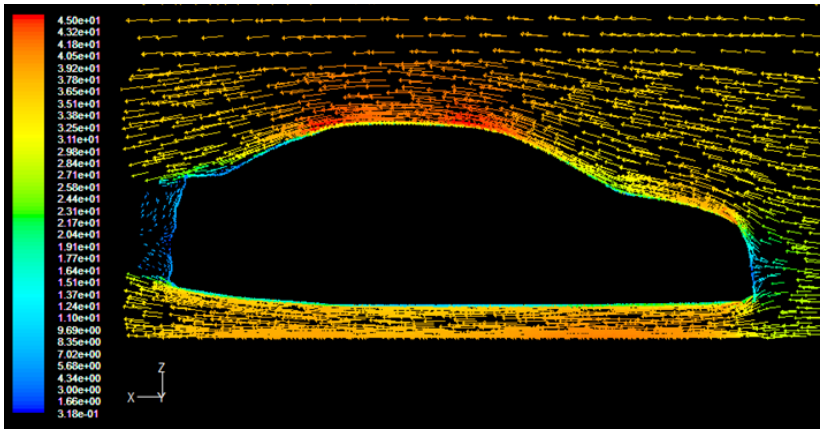

Fig14. Velocity vectors around the car presented in the mid-plane surface.

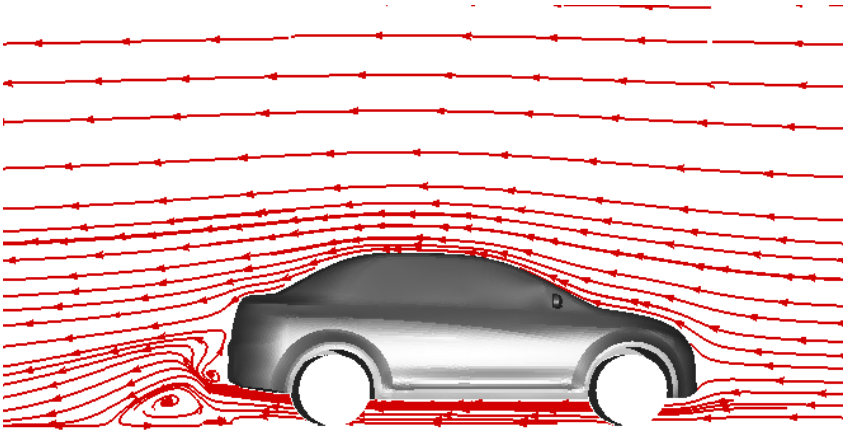

Fig15. Streamlines around the car presented in the mid-plane surface.

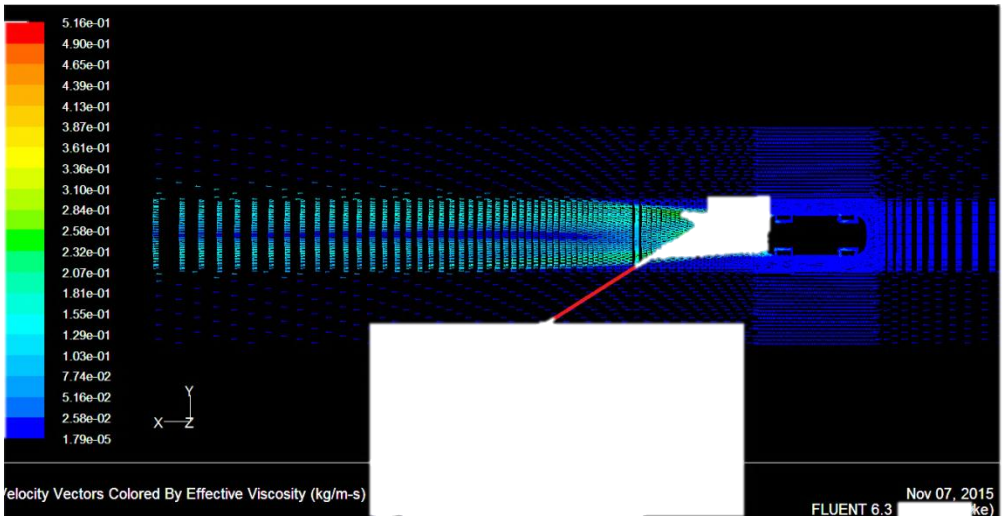

Fig16. Velocity vectors in downstream the car and the wake region.

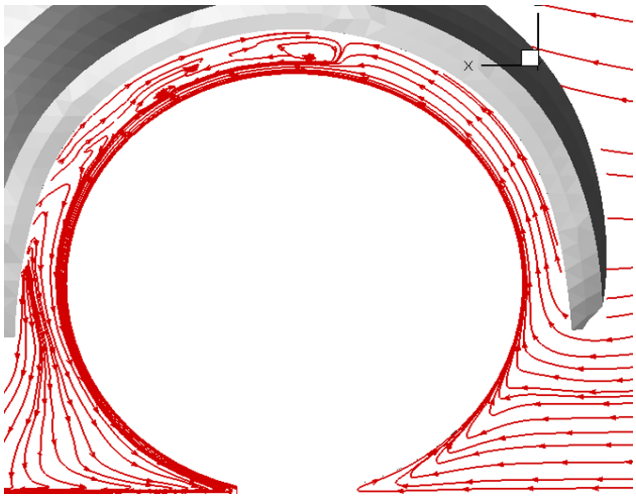

Fig17. Streamlines around the car tire.

Table 3 Aerodynamic force and moment components of the car with different flow velocities.

Velocity (mph)	D (N)	S (N)	L (N)	RM (N.m)	PM (N.m)	
60	309.11	0	106.81	0	-266.02	0
70	422.26	0	145.62	0	-362.76	0
80	546.43	0	192.38	0	-475.95	0
90	694.43	0	241.49	0	-600.07	0
100	853.54	0	295.12	0	-736.22	0

Table 4 Aerodynamic force and moment coefficients of the car with different flow velocities.

Velocity (mph)	C_d	C_s	C_l	C_{rm}	C_{pm}	C_{ym}
60	0.3211	0	0.111	0	-0.1063	0
70	0.3223	0	0.111	0	-0.1065	0
80	0.3119	0	0.112	0	-0.1069	0
90	0.3206	0	0.115	0	-0.1065	0
100	0.3192	0	0.110	0	-0.1050	0

Table 5 Aerodynamic force and moment components of the car with different yawing flow angles.

ψ	D (N)	S (N)	L (N)	RM (N.m)	PM (N.m)	YM (N.m)
0	546.43	0	192.38	0	-475.95	0
5	607.75	298.38	93.06	1559.13	-7939.30	-326.53
10	699.49	668.61	-22.06	2665.14	-9146.25	-648.91
15	726.43	979.36	-44.17	3596.34	-9470.04	-961.39
20	671.22	1262.10	-55.22	4862.70	-10270.66	-1198.89

Table 6 Aerodynamic force and moment coefficients of the car with different yawing flow angles.

ψ	C_d	C_s	C_l	C_{rm}	C_{pm}	C_{ym}
0	0.3119	0	0.112	0	-0.107	0
5	0.3552	0.1743	0.054	0.35	-1.78	-0.0734
10	0.4088	0.3907	-0.012	0.59	-2.05	-0.1453
15	0.4245	0.5723	-0.025	0.81	-2.13	-0.2161
20	0.4542	0.7451	-0.032	1.1	-2.30	-0.2694

Table 4 presents the value of non-dimensional force and moment coefficients of the above blunt bodies when Reynolds is higher than 107 [23]. For this car, Reynolds number is defined based on the wheelbase (WB) length which is 2.6 m, and for the lowest flow speed (V=60 mph) Reynolds is approximately 4.7×107.

Based on the above results, the drag and lift coefficients for all flow velocities are approximately 0.32 and 0.11, respectively.

Cross wind effect

Cross wind effect can also affect aerodynamic forces on the car and the performance of road vehicles. There are some instances in which the accident is induced by the wind effects. At 25 January 1990, in UK about 400 wind induced vehicle accidents occurred in which the most common type of them was overturning [24]. Seven high-sided road vehicles on 11 August 2004 were overturned by high winds when they were running on the Humen suspension bridge in China [2]. Different research studies have also been conducted to investigate the effect of cross winds on road vehicles [1,25], hence it's necessary to predict these effects on the car.

Cross wind effects are investigated based on the second test configuration explained in Table 1, assuming that air flows with 80 mph with a yawing angle ranging from 0 to 20 degree. Results of this test in terms of the force and moment components are outlined in Table 5.

Increasing the yaw angle has led to the increase in the drag and side forces, however the lift force decreases and becomes negative. The absolute value of all the moment components have also increased.

Table 6 represents the effect of the yaw angle on non-dimensional force and moment coefficients. Increment of the yaw angle results in increase of the drag and side force coefficients. The rate of increment of the side coefficient is even higher than the drag coefficient such that for ψ=20°, Cs becomes even higher than Cd. Comparing the lift coefficient with the other force coefficients reveals that the lift coefficient is very lower than the other force components and can be ignored in comparison with the car weight. The absolute value of moment coefficients have also increased by increasing the yaw angle.

1. Car elevation effect

As discussed in section 0, the flow streams flowing from the bottom, top and sides of the car reach to each other on the back of car trunk, and form wake regions with complex recirculating areas. As a consequence, elevation of the car ride height can affect these low pressure regions and change the value of the force and moment components. Table 7 summarizes results of the 3rd test and compares them with those of the base test configuration, with V=80 mph and ψ=0. By lowering the car ride elevation, the drag force decreases about 7%, while the variation of the lift force is not considerable. The absolute value of pitching moment has also decreased. These results are in accordance with our physical sense, because by lowering the car's height the frontal area also decreases that could lead to a lower drag force.

In contrast to the decline of drag and lift forces, their corresponding non-dimensional coefficients have slight increments which are caused by the decrement of the frontal area.

Hence, it can be concluded that lowering the car height would decrease the force and moment components while its effect on force and moment coefficients is not considerable.

Mirrors effect

Formation of wake regions on the back of mirrors can affect aerodynamic characteristics of the car. Therefore, the effect of mirrors on force and moments is determined in this section. Table 9 presents the force and moment components for the two cases with and without mirrors. Obviously, the impact of mirrors on the drag force is remarkable and removing mirrors can decrease the drag force up to 11 percent. Despite the mentioned effect on the drag force, no significant change can be observed in the lift force and pitching moment.

The force and moment coefficients for the mentioned cases and the effect of mirrors on these coefficients are described in Table 10. Although the drag force increases with removing the mirrors, its coefficient does not change, since the frontal area has also decreased. In addition, a slight increase in the lift and pitching moment coefficients has been observed.

Table 7 The effect of car's ride height on aerodynamic force and moment components of the car.

Elevation (mm)	D(N)	S (N)	L (N)	RM (N.m)	PM (N.m)	YM (N.m)
0	546.43	0	192.38	0	-475.95	0
-25	505.955	0	191.46	0	-431.154	0

Table 8 The effect of car's ride height on aerodynamic force and moment coefficients of the car.

Elevation (mm)	C_d	C_s	C_l	C_{rm}	C_{pm}	C_{ym}
0	0.3119	0	0.112	0	-0.107	0
-25	0.322	0	0.116	0	-0.0975	0

Table 9 The effect of mirrors on aerodynamic force and moment components of the car.

Mirror	D(N)	S (N)	L (N)	RM (N.m)	PM (N.m)	YM (N.m)
With	546.43	0	192.38	0	-475.95	0
Without	485.7	0	193.38	0	-473.42	0

Table 10 The effect of mirrors on aerodynamic force and moment coefficients of the car.

Mirror	C_d	C_s	C_l	C_{rm}	C_{pm}	C_{ym}
With	0.3119	0	0.112	0	-0.107	0
Without	0.315	0	0.125	0	-0.118	0

Conclusions

Computational fluid dynamics simulations are performed in order to predict the aerodynamic characteristics of the first prototype of the Iranian National Platform (NP01) in different conditions. Turbulent flow around the car is solved using the RANS equations in conjunction with the realizable k-ε model. First a validation is done and results of CFD simulation are compared with those of the Ahmed reference model with an acceptable accuracy. Next, four testing configurations have been simulated to investigate the effects of: 1- velocity; 2- cross wind; 3- car ride height; and 4- mirrors on aerodynamic forces and moments, and different aerodynamics phenomena have been discussed. Results presented in terms of pressure contours, velocity vectors, streamlines around the car, and the force and moment components. Outcomes of the present work can be concluded as follows:

Increasing the velocity of the car rises the drag and lift forces, and the pitching moment, while their corresponding non-dimensional coefficients are approximately constant and their estimated values are 0.32, 0.11 and -0.106, respectively.

Cross wind effect has a high impact on all the force and moment components, such that increasing the yaw angle leads to the increment of the drag and side forces, and the absolute value of all moment components. While the lift force for $\psi = 0$ is upward, and increasing the yaw angle causes the lift force to decline with subsequent variation of the direction of the lift force. In addition, the lift force, in comparison with the car weight, is not considerable. In this case, different force and moment coefficients have the same trend as their pertinent components.

By elevation of the car's height and decreasing its ride height up to 25 mm, the drag force decreases about 7%, while its coefficient is almost unchanged. Furthermore, the effect of car elevation on the other force and moment components and coefficients is negligible.

Mirrors have a high impact on the drag force, such that by removing them an 11% decrement in the drag force is determined. Since, by removing mirrors the frontal area decreases, hence in this case, non-dimensional coefficients have not experience a considerable change in their values.

References

[1]. Liu X, Han Y, Cai CS, Levitan M, Nikitopoulos D. Wind tunnel tests for mean wind loads on road vehicles. J Wind Eng Ind Aerodyn 2016;150:15–21. doi:10.1016/j.jweia.2015.12.004.

[2]. Zhu LD, Li L, Xu YL, Zhu Q. Wind tunnel investigations of aerodynamic coefficients of road vehicles on bridge deck. J Fluids Struct 2012;30:35–50. doi:10.1016/j.jfluidstructs.2011.09.002.

[3]. Kieffer W, Moujaes S, Armbya N. CFD study of section characteristics of Formula Mazda race car wings. Math Comput Model 2006;43:1275–87. doi:10.1016/j.mcm.2005.03.011.

[4]. Browand F, McCallen R, Ross J, editors. The Aerodynamics of Heavy Vehicles II: Trucks, Buses, and Trains. vol. 41. Berlin, Heidelberg: Springer Berlin Heidelberg; 2009.

[5]. McCallen R, Browand F, Ross J, editors. The Aerodynamics of Heavy Vehicles: Trucks, Buses, and Trains. vol. 19. Berlin, Heidelberg: Springer Berlin Heidelberg; 2004.

[6]. Dillmann A, Orellano A, editors. The Aerodynamics of Heavy Vehicles III. vol. 79. Cham: Springer International Publishing; 2016.

[7]. Wilcox DC. Turbulence Modeling for CFD. 3rd edition. La Cãnada, Calif: D C W Industries; 2006.

[8]. Launder BE, Spalding DB. Lectures in mathematical models of turbulence. London; New York: Academic Press; 1972.

[9]. Yakhot V, Orszag SA. Renormalization group analysis of turbulence. I. Basic theory. J Sci Comput 1986;1:3–51. doi:10.1007/BF01061452.

[10]. Shih T-H, Liou WW, Shabbir A, Yang Z, Zhu J. A new k-ϵ eddy viscosity model for high reynolds number turbulent flows. Comput Fluids 1995;24:227–38. doi:10.1016/0045-7930(94)00032-T.

[11]. Blocken B, Toparlar Y. A following car influences cyclist drag: CFD simulations and wind tunnel measurements. J Wind Eng Ind Aerodyn 2015;145:178–86. doi:10.1016/j.jweia.2015.06.015.

[12]. Murad N, Naser J, Alam F, Watkins S. Computational fluid dynamics study of vehicle A-pillar aero-acoustics. Appl Acoust 2013;74:882–96. doi:10.1016/j.apacoust.2012.12.011.

[13]. Wang JY, Hu XJ. Application of RNG k-ε Turbulence Model on Numerical Simulation in Vehicle External Flow Field. Appl Mech Mater 2012;170-173:3324–8.

[14]. Ahmed S, Ramm G, Faltin G. Some Salient Features Of The Time-Averaged Ground Vehicle Wake. SAE Trans Pap 840300 n.d. doi:doi:10.4271/840300.

[15]. Bella G, Krastev VK. On the RANS Modeling of Turbulent Airflow Over a Simplified Car Model 2011:871–83. doi:10.1115/AJK2011-23006.

[16]. Singh SN, Rai L, Puri P, Bhatnagar A. Effect of moving surface on the aerodynamic drag of road vehicles. Proc Inst Mech Eng Part J Automob Eng 2005;219:127–34. doi:10.1243/095440705X5886.

[17]. Kang SO, Jun SO, Park HI, Song KS, Kee JD, Kim KH, et al. Actively translating a rear diffuser device for the aerodynamic drag reduction of a passenger car. Int J Automot Technol 2012;13:583–92. doi:10.1007/s12239-012-0056-x.

[18]. McManus J, Zhang X. A Computational Study of the Flow Around an Isolated Wheel in Contact With the Ground. J Fluids Eng 2005;128:520–30. doi:10.1115/1.2175158.

[19]. Tien Phuc Dang, Zhengqi Gu, Zhen Chen. Numerical simulation of flow field around the race car in case: Stationary wheel and rotating wheels. Int J Numer Methods Heat Fluid Flow 2015;25:1896–911. doi:10.1108/HFF-04-2014-0107.

[20]. Patankar SV. Numerical Heat Transfer and Fluid Flow. New York: Taylor & Francis; 1980.

[21]. Ahmed SR. Influence of Base Slant on the Wake Structure and Drag of Road Vehicles. J Fluids Eng 1983;105:429–34. doi:10.1115/1.3241024.

[22]. Beaudoin J-F, Aider J-L. Drag and lift reduction of a 3D bluff body using flaps. Exp Fluids 2008;44:491–501. doi:10.1007/s00348-007-0392-1.

[23]. White F. Fluid Mechanics. 8th ed. New York: McGraw-Hill Education; 2016.

[24]. Baker CJ, Reynolds S. Wind-induced accidents of road vehicles. Accid Anal Prev 1992;24:559–75. doi:10.1016/0001-4575(92)90009-8.

[25]. Guilmineau E, Chikhaoui O, Deng G, Visonneau M. Cross wind effects on a simplified car model by a DES approach. Comput Fluids 2013;78:29–40. doi:10.1016/j.compfluid.2011.08.020.